This document was prepared in conjunction with work accomplished under Contract No. DE-AC09-96SR18500 with the U.S. Department of Energy.

DETERMINATION OF CONSTRAINT-MODIFIED J-R CURVES FOR CARBON STEEL STORAGE TANKS

P.-S. Lam, Savannah River Technology Center, Westinghouse Savannah River Company, Aiken, South Carolina 29808
Y.J. Chao, X.-K. Zhu, Y. Kim
Department of Mechanical Engineering, University of South Carolina, Columbia, South Carolina 29208
R. L. Sindelar, Savannah River Technology Center, Westinghouse Savannah River Company, Aiken, South Carolina 29808

Abstract

Mechanical testing of A285 carbon steel, a storage tank material, was performed to develop fracture properties based on the constraint theory of fracture mechanics. A series of single edge-notched bend (SENB) specimen designs with various levels of crack tip constraint were used. The variation of crack tip constraint was achieved by changing the ratio of the initial crack length to the specimen depth. The test data show that the J-R curves are specimen-design-dependent, which is known as the constraint effect. A two-parameter fracture methodology is adopted to construct a constraint-modified *J-R* curve, which is a function of the constraint parameter, A_2, while J remains the loading parameter. This additional fracture parameter is derived from a closed form solution and can be extracted from the finite element analysis for a specific crack configuration. Using this set of SENB test data, a mathematical expression representing a family of the J-R curves for A285 carbon steel can be developed. It is shown that the predicted *J-R* curves match well with the SENB data over an extensive amount of crack growth. In addition, this expression is used to predict the J-R curve of a compact tension specimen (CT), and good agreement to the actual test data is achieved. To demonstrate its application in a flaw stability evaluation, a generic A285 storage tank with a postulated axial flaw is used. For a flaw length of 10% of the tank height, the predicted J-R curve is found to be similar to that for a SENB specimen with a short notch, which is in a state of low constraint. This implies that the use of a J-R curve from the ASTM (American Society for Testing and Materials) standard designs, which typically are high constraint specimens, may be overly conservative for analysis of fracture resistance of large structures.

Introduction

Ductile fracture in engineering materials is usually characterized by the fracture initiation toughness J_{IC} and the subsequent fracture resistance curve (i.e., *J-R* curve). For a cracked component or structure, the J_{IC} dictates *when* the crack propagation is initiated, and the *J-R* curve determines *how far* the crack can grow in a stable manner at an applied load characterized by *J*. These single-parameter fracture criteria, namely, the J_{IC} and the *J-R* curve, have been widely used in fracture analyses of engineering structures when the

ductile tearing is dominant. Therefore, the J_{IC} and the *J-R* curves obtained from the laboratory specimens must be reasonably accurate and applicable to the full-scale structures. This concept is termed "transferability."

The single-parameter fracture toughness and the fracture resistance properties presently used in these fracture analyses, however, are known to be dependent of test specimen design. This dependency is often referred to the effect of crack tip constraint. The fracture toughness data are generally obtained from standard specimens, such as those specified by ASTM Standard Test Method for Measurement of Fracture Toughness (E 1820). It is commonly accepted that the standard specimens in the laboratory testing are typically of high constraint, while nonstandard specimens and actual cracked structures may be under low constraint configurations. Accordingly, the constraint effect on the *J-R* curve must be considered when it is applied to a structure in service for flaw stability evaluation.

In general, the fracture initiation toughness J_{IC} and the *J-R* curve could be functions of test specimen geometry and loading configurations. In recent years, many researchers studied, experimentally and analytically, the constraint effect on the fracture properties for both brittle and ductile materials. For example, Hancock et al. [1] measured the fracture toughness J_{IC} and *J-R* curves of the ASTM 710 Grade A steel using three point bend (TPB), compact tension (CT), center cracked panel (CCP) in tension and surface cracked panel (SCP) in tension with various crack depths. Joyce and Link [2,3] presented their experiment data of ductile crack extension for specimens such as TPB, CT, single edge-notched bend (SENB), single edge-notched tensile (SENT), and double edge-cracked plate (DECP) in tension with shallow to deep cracks for A533B, HY-100 and HY-80 structural steels. These researchers did not find a significant constraint effect on the fracture initiation toughness J_{IC}, but they observed apparent and replicable changes in the slopes of the *J-R* curves after certain amount of crack growth. Similar results were reported by Marschall et al. [4], Eisele et al. [5], Roos et al. [6], Henry et al. [7] and Haynes and Gangloff [8] for CCP, CT, DECP, SENB and SENT testing with various specimen sizes. All experimental data reported in literature seem to suggest that the *J-R* curves may depend on the level of constraint. Qualitatively, at a fixed crack extension (Δa), the value of the J-integral of a high constraint specimen is less than that of a low constraint specimen. In other words, the low constraint specimen exhibits higher load carrying capacity.

To validate the experimental results of the ductile crack growth, two-dimensional and three-dimensional finite element analyses (FEA) were performed by many researchers, such as Yuan and Brocks [9], Brocks et al. [10], Henry et al. [7], Kikuchi [11], and Yan and Mai [12]. Most of these studies used the J_2 flow theory of plasticity for material response idealization, and input the experimental applied load or the load-line displacement to the finite element models of various fracture specimens, including CT, TPB, SENB, SENT and CCP. The numerical results are consistent with the experimental observations. The results show that (i) ductile crack growth is sensitive to the crack-tip constraint and the amount of *J*-controlled crack growth varies with specimen design, (ii) upon crack initiation, the fracture toughness J_{IC} increases slightly with decreasing crack length or, equivalently, lower

crack-tip constraint, and (iii) during crack growth, the ductile tearing resistance increases with decreasing constraint level or triaxiality.

Based on the experimental data, FEA results and the J-A_2 crack tip solutions provided by Yang et al. [13,14] and Chao, et al. [15], a new methodology has been proposed for constructing a constraint-modified J-R curve, using the A_2 as the constraint parameter. The details of this methodology can be found in Chao and Zhu [16] and Chao et al. [17]. As discussed by Nikishkov et al. [18] and Chao and Zhu [19], the J-A_2 three-term solution [13-15] is considered as the most effective and theoretically sound asymptotic solution. As a result, the three-term solution has been extensively applied to the following areas: 1) fracture toughness evaluation (Chao and Ji, [20], and Chao and Lam [21]); 2) specimen size requirements in two-parameter fracture testing (Chao and Zhu [19]); 3) non-hardening materials (Zhu and Chao [22]); 4) creeping materials (Chao et al., [23]); 5) three dimensional cracks (Kim et al. [24]); and 6) ductile crack growth (Chao and Zhu [16], and Chao et al. [17]). Other approaches to quantify the crack tip constraint include the J-T technique proposed by Betegon and Hancock [25], and the J-Q theory by O'Dowd and Shih [26,27].

The objective of this paper is to use the J-A_2 methodology to construct a general expression for a constraint-modified J-R curve for the A285 carbon steel. With the test data from a set of SENB specimens, the fracture initiation toughness J_{IC} and the J-integral values at the crack extension of 1.5 mm or 3 mm (denoted by $J_{1.5mm}$ or J_{3mm}, respectively) were determined. The values of A_2 were obtained by comparing the FEA result of each specimen to the J-A_2 analytical solution. The functional dependencies of J_{IC}, and $J_{1.5mm}$ (or J_{3mm}) on the constraint parameter A_2, were then established. Using the power-law relationship suggested by the ASTM E 1820, the constraint-modified J-R curve for A285 carbon steel can be constructed. Comparisons of the predicted J-R curve with the experimental data of each specimen show a good match over a relatively large crack extension.

The resulting constraint modified J-R curve based on SENB test data is used to predict the J-R curve based on a standard CT specimen design. The A_2 value of the CT specimen is estimated with the FEA and then substituted into the general expression. The predicted J-R curve is shown to have good agreement with the experimental curve from testing the CT specimen. The application of this methodology is further demonstrated in the case of an axial flaw in the sidewall of an A285 carbon steel storage tank. A three-dimensional finite element model is constructed for the flawed tank, and the corresponding A_2 value is calculated. It can be shown that the predicted J-R curve, suitable for the storage tank geometry, is very closed to the J-R curves obtained earlier from a SENB specimen with a short notch (low constraint). Therefore, it can be concluded that the use of a J-R curve determined from standard specimen testing (normally in high constraint configurations) may be overly conservative for the fracture resistance of large structures.

Specimen Design and Experimental Results

Specimen Design and Material Properties. The ASTM E 1820 specified SENB dimensions were used, except for the initial crack lengths that were varied to promote different levels of crack tip constraint. The specimen thickness B is 15.875 mm (0.625 inches) with 10% side groove on each side, the width W is 31.75 mm (1.25 inches), the length L is 142.88 mm (5.625 inches), and the span S is 127 mm (5 inches). The initial crack depth to the width ratios (a/W) are, respectively, 0.32 (Specimen 1D), 0.35 (Specimen 2C), 0.59 (Specimen 2A), and 0.71 (Specimen 4C).

The material used for testing is A285 carbon steel. A standard tensile specimen from the heat of steel used to machine both the SENB and the CT specimens was tested. The tensile test results show that the 0.2% offset yield stress of this steel is 251 MPa (36.4 ksi), the ultimate tensile stress 415 MPa (60.2 ksi), the Young's modulus (E) 207 GPa (30,000 ksi), and the strain hardening exponent 5. The effective yield stress or the flow stress, defined as the average of the 0.2% offset yield stress and the ultimate tensile stress, is thus 333 MPa (48.3 ksi). The Poisson ratio for this material is 0.3.

Experimental J-R Curves of A285 Steel. The experimental results of the J-R curves are shown in Figure 1. The test data of the SENB Specimen 2C are not used in this work due to the cleavage interruption. The current study is focused on the stable crack growth in mild steels such as A285 under ductile fracture conditions, that is, above the ductile-to-brittle transition temperature. Figure 1 also includes the J-R curve from the test results using a standard CT specimen design. This J-R curve will be compared to the predicted curve, which is formulated with the SENB test data. This CT specimen was tested in a previous experimental program using material cut from the same steel plate as the SENB specimens. Therefore, identical material was used and the only difference is the test specimen design. The width (W) of the CT specimen is 63.58 mm (2.50 inches) and the a/W ratio is 0.47. The specimen height is 48.87 mm (1.92 inches) and its thickness (B) of the is identical to the SENB specimens, that is, 15.875 mm (0.625 inches) with 10% side groove on each side.

Determination of Fracture Toughness J_{IC}. The test data of Specimens 1D, 2A, and 4C were used for the development of a constraint modified J-R curve. The procedure described in ASTM E 1820 is used to estimate the initiation fracture toughness, namely, J_{IC}. The calculation of an interim J_Q is stated in A9.6 of E 1820 and is illustrated in Figures 2 to 4, respectively, for Specimens 1D, 2A, and 4C. The exclusion lines at 0.15, 0.2, and 1.5 mm crack extension (Δa) are defined respectively by the following equations: $J = 666(\Delta a - 0.15)$, $J = 666(\Delta a - 0.2)$, and $J = 666(\Delta a - 1.5)$, where J is in kJ/m^2 and Δa is in millimeters. The J limit lines (J_{limit}), as defined in ASTM E 1820, are also shown in Figures 2 to 4. The values of J_{limit} are 479, 289, and 204 kJ/m^2, respectively, for cases of a/W equal to 0.32, 0.59 and 0.71.

In the case of the shallow crack SENB (a/W= 0.32), Figure 2 shows that there are acceptable data points bounded by the 0.15 mm exclusion, the J limit line and the 1.5 mm

exclusion line(solid symbols in Figure 2). These acceptable data points can be represented by a power-law expression, that is $J_{acc} = 412.544(\Delta a)^{0.751}$ kJ/m^2. The intersection of this power law curve and the 0.2 mm exclusion line defines $J_Q = 297.29$ kJ/m^2 for this specimen (a/W = 0.32). However, both the ligament size ($b_0 = 21.59$ mm) and the thickness ($B = 15.88$ mm) do not satisfy the specimen size requirement of ASTM E 1820, that is, B or b_0 must be greater than $25J_Q / \sigma_y$, which is 22.32 mm in this case. Based on ASTM E 1820, this interim J_Q does not exactly meet the criterion for J_{IC}. Nevertheless, for the scope of this work, it is approximated that $J_{IC} \approx J_Q = 297.29$ kJ/m^2.

Similar process is performed for the other two SENB specimens (a/W = 0.59 and 0.71). No valid data points can be found to satisfy ASTM E 1820. The criterion is modified so the data between the 0.15 and the 1.5 mm exclusion lines are considered acceptable. The power law curve expressions for the "acceptable" data are $J_{acc} = 392.586(\Delta a)^{0.601}$, and $J_{acc} = 341.568(\Delta a)^{0.606}$ kJ/m^2, respectively, for Specimens 2A and 4C. As in the case of Specimen 1D, these two specimens do not satisfy the size requirement of ASTM E 1820. Therefore, by approximation the corresponding values of J_{IC} are, respectively, 305.46 and 240.65 kJ/m^2.

Numerical Computation and Constraint Analysis

FEA Modeling. The finite element method is used to calculate the stress and strain fields in the test specimens and determine the fracture parameters. The parameter A_2 is extracted from the stress distribution around the crack tip when the loading of the specimen reaches the initiation fracture toughness (J_{IC}), at which A_2 attains a nearly constant value.

The finite element models were built for the SENB specimens with various a/W ratios (i.e., 0.32, 0.59 and 0.71). The typical fracture mechanics mesh focusing to the crack tip is used. Due to symmetry, only one-half of the specimen is modeled. Each model contains 945 eight-noded plane strain elements and 2976 nodes. The smallest element size is 3.45×10^{-3} mm. Similar finite element mesh was built for the CT specimen (a/W= 0.47), for which the experimental J-R curve is known and is used as an indicator to demonstrate the predictability of the proposed constraint effect methodology.

The material response is modeled by the deformation theory of plasticity within the small strain framework. The stress-strain relation follows the Prandl-Reuss constitutive equation:

$$\frac{\varepsilon_{ij}}{\varepsilon_0} = (1+\upsilon)\frac{\sigma_{ij}}{\sigma_0} - \upsilon\frac{\sigma_{kk}}{\sigma_0}\delta_{ij} + \frac{3}{2}\alpha\left(\frac{\sigma_e}{\sigma_0}\right)^{n-1}\frac{s_{ij}}{\sigma_0} \qquad (1)$$

where σ_0 is the initial yield stress, ε_0 is defined as $\varepsilon_0 = \sigma_0 / E$, υ is the Poisson ratio, n is the strain-hardening exponent, α is the Ramberg-Osgood parameter (yield offset), $s_{ij} = \sigma_{ij} - \sigma_{kk}\delta_{ij}/3$ is the deviatoric stress, and $\sigma_e = (3s_{ij}s_{ij}/2)^{1/2}$ is the Mises equivalent stress. For the A285 carbon steel used in fracture testing, the material constants are taken as $\sigma_0 = 251$ MPa, $E = 207$ GPa, $\upsilon = 0.3$, $n = 5$ and $\alpha = 3.2$.

Determination of Constraint Parameter A_2. The J-A_2 three-term solution (Yang et al., [13,14] and Chao et al., [15]) is to characterize the crack-tip fields for all specimens considered (SENB and CT). The asymptotic stress solution near the crack tip for a power law material can be written as

$$\frac{\sigma_{ij}}{\sigma_0} = A_1\left[\left(\frac{r}{L}\right)^{s_1}\tilde{\sigma}_{ij}^{(1)}(\theta) + A_2\left(\frac{r}{L}\right)^{s_2}\tilde{\sigma}_{ij}^{(2)}(\theta) + A_2^{\,2}\left(\frac{r}{L}\right)^{s_3}\tilde{\sigma}_{ij}^{(3)}(\theta)\right] \tag{2}$$

where the angular functions $\tilde{\sigma}_{ij}^{(k)}$ (k= 1, 2, or 3) and the stress singularity exponents s_k ($s_1 < s_2 < s_3$) are functions of the hardening exponent n and the applied loads, and are independent of the other material constants (i.e. α, ε_0, and σ_0). In the above equation, L is a characteristic length parameter and set to 1 mm throughout this work. The parameters A_1 and s_1 are related to the Hutchinson-Rice-Rosengren (HRR) field [28-30] by

$$A_1 = \left(\frac{J}{\alpha\varepsilon_0\sigma_0 I_n L}\right)^{-s_1}, \qquad s_1 = -\frac{1}{n+1} \tag{3}$$

and $s_3 = 2s_2 - s_1$ for $n \geq 3$. The parameter A_2 is an undetermined function which may be related to the loading and geometry of the specimen. The plane strain Mode I dimensionless functions $\tilde{\sigma}_{ij}^{(k)}$, $\tilde{\varepsilon}_{ij}^{(k)}$, $\tilde{u}_i^{(k)}$, s_k and I_n have been calculated and tabulated by Chao and Zhang [31]. It can be seen that Equation (2) is the HRR stress solution when $A_2 = 0$.

For all the specimens considered in this paper, it can be shown that A_2 becomes a constant, or location-independent, within the range $r\sigma_0 / J < 0.5$. Therefore, the A_2 values are obtained by matching the opening stress from the three-term solution to the FEA results at $r\sigma_0 / J \approx 0.2$ from the crack tip. As a result, the values of A_2 for the SENB specimens are, respectively, -0.3609, -0.3019, and –0.2712, for a/W ratios 0.32, 0.59 and 0.71. In the case of the CT specimen (a/W= 0.47), the value of A_2 was determined as –0.2099. The stress distributions of i) FEA results; ii) the J-A_2 asymptotic solutions; and iii) the HRR

plane strain solution, are plotted in Figure 5 within the range of $r\sigma_0 / J < 1$. It can be seen that the three-term J-A_2 solutions with these A_2 values match well with the FEA results. On the other hand, the HRR solution tends to overestimate the opening stresses for SENB and CT specimens considered in this study. This indicates that the use of single fracture parameter (J) may be insufficiently to characterize the stress fields near the crack tip when general yielding occurs.

Constraint-modified J-R Curves of A285 Steel

Methodology. Similar to the concept of *J*-controlled crack growth, Chao and Zhu [16] and Chao et al. [17] have developed a *J-A*$_2$ controlled crack growth by extending the *J-A*$_2$ two-parameter description for stationary cracks to the case of growing cracks under small crack extension. They applied the *J-A*$_2$ description to the analysis of ductile crack growth, and proposed an engineering methodology to quantify the constraint effect on the *J-R* curves.

As pointed out by Chao and Zhu [17], under large-scale yielding or near fully plastic deformation, the constraint parameter A_2 determined at the fracture initiation load, $J = J_{IC}$, remains unchanged for subsequent stable crack growth ($J \geq J_{IC}$). Therefore, when small crack extension occurs within the *J-A*$_2$ dominant region, the value of A_2 can be considered as a constant. Under *J-A*$_2$ controlled crack growth, the curve of *J* versus crack extension, Δa, can be expressed by a power law relationship, as suggested by ASTM E 1820:

$$J(\Delta a, A_2) = C_1(A_2)\left(\frac{\Delta a}{k}\right)^{C_2(A_2)} \tag{4}$$

where $k = 1\,\text{mm}$, and the coefficients $C_1(A_2)$ and $C_2(A_2)$ are to be determined, respectively, as the functions of *A*$_2$. Note that C_1 and C_2 are constants in the original ASTM E 1820 formulation (A_2= 0).

Equation (4) extends the current ASTM *J-R* curve concept, $J(\Delta a)$, to a constraint-modified *J-R* curve $J(\Delta a, A_2)$. Therefore, the objective of this methodology is to construct the functional dependencies of C_1 and C_2 on the constraint parameter A_2. Once the functional forms of $C_1(A_2)$ and $C_2(A_2)$ are known, the family of constraint-modified *J-R* curves is completely determined.

Note that equation (4) contains two unknown variables, C_1 and C_2 for a given A_2. At least two equations are needed to solve for these values. The first equation can be set up when J= J_{IC}. At that loading level the A_2 value will become unchanged due to the fully plastic condition around the crack tip. According to ASTM E 1820, J_{IC} is defined as the *J* at crack extension $\Delta a = \Delta a_Q = J_{IC} / 2\sigma_y + 0.2\,(\text{mm})$ or

$$J_{IC}(\Delta a) = J(\Delta a_Q)\Big|_{\Delta a_Q = \frac{J_{IC}}{2\sigma_y} + 0.2\,(\text{mm})} \tag{5}$$

where σ_y is the effective yield stress, defined as the average of the 0.2% yield stress and the ultimate stress. The second equation (needed to solve for C_1 and C_2) can be obtained by choosing another point on the J-R curve beyond crack initiation. The corresponding crack extension is denoted by Δa_i. Therefore, the set of simultaneous equations is

$$\begin{aligned} J\Big|_{\Delta a_Q} &= J_{IC}(A_2) \\ J\Big|_{\Delta a_i} &= J_{\Delta a_i}(A_2) \end{aligned} \tag{6}$$

In principle, if Δa_i is chosen between 0.5 and 2 mm, it automatically satisfies the ASTM E 1820 criterion for the acceptable data. However, if the specimen exhibits much longer crack extension (Δa_i > 2 mm), choosing Δa_i outside of that range may yield a better fit for the overall J-R curve. This practice is adopted in the next section for constructing the constraint-modified J-R curve for A285 carbon steel.

Substituting equation (6) into (4), the following two equations are sufficient to solve for C_1 and C_2:

$$\begin{aligned} C_1(A_2)\left(\frac{J_{IC}}{2k\sigma_y} + 0.2\right)^{C_2(A_2)} &= J_{IC}(A_2) \\ C_1(A_2)(\Delta a_i)^{C_2(A_2)} &= J_{\Delta a_i}(A_2) \end{aligned} \tag{7}$$

Equations (7) are nonlinear in C_1 and C_2 for a given A_2 and must be solved numerically. The valid range of A_2, based on past studies, is between -1 and 0, as the crack tip constraint varies from low to high. Solving C_1 and C_2 for a series of A_2 values within this range ($-1 \le A_2 \le 0$) will give the functional dependencies of C_1 and C_2 with respect to A_2. Finally, regression analysis or curve fitting will provide the desired functional forms of C_1 and C_2, respectively, in terms of the constraint parameter A_2.

For a given material, once the expression of the constraint-modified *J-R* curve, or equation (4), is obtained, the *J-R* curve can be accurately determined for any specific cracked geometry (e.g., non-ASTM specimens or actual structural members), provided that the constraint parameter A_2 for that cracked geometry is known.

Construction of A285 Constraint-modified J-R Curve. Using the SENB test data and the methodology described in the last section, a constraint-modified *J-R* curve in term of A_2 can be constructed for A285 carbon steel. Two equations are set up to solve for C_1 and C_2 at J= J_{IC} and J= $J_{1.5mm}$. Note that $J_{1.5mm}$ is near the center of the acceptable test data ($\Delta a = 1.5\,\text{mm}$) specified by ASTM E 1820.

The J_{IC} parameter is less sensitive to the specimen geometry. A single valued J_{IC} is approximately chosen (by least squares) for the SENB test data:

$$J_{IC} = 281.13\ \text{kJ/m}^2 \text{ at } \Delta a_{J_{IC}} \cong 0.6221\,\text{mm}. \tag{8}$$

A straight line is used to linearly fit the relationship of $J_{1.5mm}$ versus A_2. Therefore,

$$J_{1.5mm} = -\,1315.924\,A_2 + 89.313\ \text{kJ/m}^2 \tag{9}$$

Using the effective yield stress of A285 ($\sigma_y = 333\,MPa$) and substituting equations (8) and (9) into (7), the simultaneous equations for C_1 (A_2) and C_2 (A_2) are

$$\begin{cases} C_1(0.6221)^{C_2} = 281.13 \\ C_1 1.5^{C_2} = -1315.924 A_2 + 89.313 \end{cases} \tag{10}$$

Numerical methods, such as the nonlinear Newton iteration method, can be used to solve equation (10) for a number of A_2 values within its valid range ($-1 \le A_2 \le 0$). Linear fit to the resulting data points (numeric pairs of C_1 vs. A_2 and C_2 vs. A_2) yields

$$\begin{aligned} C_1(A_2) &= -451.452 A_2 + 239.486 \\ C_2(A_2) &= -2.058 A_2 + 0.031 \end{aligned} \tag{11}$$

Finally, the constraint-modified *J-R* curve for A285 carbon steel is obtained by substituting equation (11) to equation (4):

$$J(\Delta a,\ A_2) = (-451.452 A_2 + 239.486)\left(\frac{\Delta a}{1\,\text{mm}}\right)^{(-2.058 A_2 - 0.031)} \tag{12}$$

Alternatively, equation 9 can be replaced by selecting another value of crack extension (beyond crack initiation) on the J-R curve. Figure 1 shows that the A285 carbon steel is capable of exhibiting at least 4 mm of crack extension for the SENB and CT specimens considered in this paper. Therefore, following the same procedure but choosing $\Delta a_i = 3\,\text{mm}$, the constraint-modified J-R curve becomes

$$J(\Delta a,\ A_2) = (-277.278 A_2 + 282.203)\left(\frac{\Delta a}{1\,\text{mm}}\right)^{(-1.436 A_2 + 0.108)} \tag{13}$$

Equation (13) indeed shows better match with the SENB experimental J-R curves at large crack extension regime because the data point at $\Delta a_i = 3\,\text{mm}$ (versus 1.5 mm) was used. The predicted J-R curves are plotted against the experimental data in Figure 6, for the three SENB specimens and the CT specimen. It should be noted that only two test data points (i.e., at $\Delta a_{J_{IC}}$ and at $\Delta a_i > \Delta a_{J_{IC}}$) are needed in this methodology, and yet the predictions (Figures 6) match well with the experimental data that exceed 5 mm crack extension. This indicates that the *J*-A_2 description is capable of predicting the *J*-resistance at larger amount of crack growth.

The prediction of the CT test data is reasonable well up to about 3 mm crack extension. The deviation in the large crack growth regime is likely caused by a possible inaccuracy due to extrapolation, that is, the A_2 value (-0.2099) in the CT specimen is outside the A_2 range (-0.3609, -0.3019, and -0.2712) used to develop equation (13).

Application to A285 Carbon Steel Storage Tanks

The methodology of constructing a constraint-modified J-R curve was introduced in the last section. It has been shown that the predicted J-R curves agree well with the experimentally determined J-R curve for various specimen designs (SENB and CT) with a range of crack tip constraint. To demonstrate the application in the area of structural integrity assessment, a large A285 carbon steel storage tank with an axial flaw is used. A three-dimensional FEA is performed to extract the parameter A_2 for the storage tank. This A_2 value is then substituted into equation (13). The resulting J-R curve is suitable for evaluating the crack growth characteristics of the axial flaw in the storage tank.

Finite Element Analysis. An A285 carbon steel cylindrical storage tank under uniform internal pressure is considered. The radius of the tank is 11.43 m (37.5 ft), the height (2H) is 7.468 m (24.5 ft), and the sidewall plate thickness (t) is 12.7 mm (0.5 in.). A throughwall crack in the axial direction of the tank is assumed to exist. The crack length is 10% of the tank height (a/H= 0.1). Due to symmetry only one quarter of the cylindrical tank is modeled with the finite elements (Figure 7). A coordinate system is employed such that the *x*-axis lies in the radial direction of the tank and coincides with the straight crack front, the *z*-axis is axial direction of the tank and the *y*-axis is perpendicular to the crack plane.

The 20-noded quadratic brick elements with reduced integration are used throughout the model, with 30 elements in the radial direction and biased towards the crack tip so the element size is gradually increased with the radial distance from the crack. The near crack tip annular region is divided by 12 sectors. To gain insight of the stress and the J-integral variation across the sidewall plate, six element-layers are designed in the thickness direction. The thickness of the element layer is exponentially reduced from the mid-plane

toward the inside or outside surfaces of the tank (i.e., 0.05t, 0.15t, 0.3t, 0.3t, 0.15t, and 0.05t). The length of the smallest element is 9.3×10^{-3} of the tank thickness. The total number of elements is 6408 with 30,869 nodes.

The internal pressures are applied to the three-dimensional finite element model. The J-integral is evaluated along the crack front across the thickness of the sidewall. It was found that the J-integral reaches a maximum value in the center plane (i.e., in the mid-section of the sidewall plate). This finding indicates that the crack initiation is most likely to occur first in the middle of the steel plate for an axial throughwall crack loaded mainly by the hoop stress. This observation is not available if a shell element model is used. It can be shown that the J-integral calculated with a previous shell element model by Lam [32] is the averaged value along the crack front.

Predicted J-R Curve for Storage Tank. The near crack tip stress distribution calculated in the center plane of the tank sidewall plate is used to determine the constraint parameter A_2, along with the J-A_2 solution (equation 2), in which the characteristic length (L) is set to 1 mm. Figure 8 shows the A_2 variations with respect to the pressure loading as well as to the J-integral that is calculated in the center plane of the tank sidewall where the maximum value is observed along the crack front. It can be seen that A_2 approaches a constant value when the internal pressure (P) is greater than 5 psi (0.034 MPa), which implies that a large scale yielding condition has occurred near the crack tip. The A_2 value is estimated as –0.3611 at the crack initiation load (J_{IC} = 281.13 kJ/m^2) when the internal pressure is 15.34 psi (0.1057 MPa). Figure 9 shows the crack opening stress distribution ($\sigma_{\theta\theta}$ at θ= 0) between the crack tip and 5J/σ_o as the internal pressure is at 15 psi (0.1034 MPa). It can be seen that very close agreement is achieved between the finite element result and the asymptotic solution with the A_2 value given as -0.3606, which is determined exactly at P= 15 psi and is slightly different from the value at crack initiation. For practical purpose, the A_2 value for the storage tank with an axial flaw of a/H= 0.1 is taken as -0.3611.

Substituting –0.3611 for A_2 in equation (13), the constraint-modified J-R curve is obtained for the A285 carbon steel storage tank with a throughwall axial flaw (a/H= 0.1):

$$J = 382.328\Delta a^{0.627}$$

in which J is in kJ/m^2 and Δa is in millimeter. This J-R curve is plotted in Figure 10 along with the predicted curves for SENB and CT specimens. As suggested by the nearly identical A_2 values, the J-R curve for the storage tank almost coincides with the SENB curve with a/W= 0.32, a relatively shallow crack specimen for SENB, which has a lower constraint than the standard specimens.

Conclusions

A group of SENB specimens with various notch lengths (a/W ratios) were tested for the crack resistance curves (J-R) for the A285 carbon steel. The experimental J-R curves show strong specimen size dependent, namely, the crack tip constraint effect. Based on the J-A_2 controlled crack growth methodology developed by Chao and Zhu [16] and Chao et al. [17] for ductile materials, the constraint effect on the J-R curves can be quantified. A mathematical expression is developed for the constraint-modified J-R curve, which is a function of the constraint parameter, A_2. This mathematical expression is in the form of a power law consistent with the ASTM E 1820. As a result, if the A_2 value is determined for a flawed structure, or a nonstandard specimen, etc., the corresponding J-R curve suitable for this geometric configuration can be immediately calculated by substituting the A_2 value to that power law expression.

The current formulation has been proven viable in predicting the J-R curves for the SENB and CT specimens. Only two J-integral levels are used in developing the functional form of the J-R curve, and yet the prediction is reliable for large amount of crack extension. It is believed that the accuracy of prediction would be further improved if a specimen with very low crack tip constraint (e.g., an SENB specimen with very a shallow notch) were tested and used in developing equation (13).

A three-dimensional finite element model simulating a carbon steel storage tank with an axial throughwall flaw is used to demonstrate its application in a fracture analysis for structural integrity assessment. The length of the flaw is postulated to be 10% of the tank height. The constraint parameter A_2 is extracted from the finite element result, and is then substituted in the power law expression. The resulting constraint-modified J-R curve for the storage tank configuration is shown to be similar to the J-R curve of a SENB specimen with a short initial notch, which is in a state of low constraint. This implies that the use of a J-R curve from the ASTM standard designs, which typically are high constraint specimens, may be overly conservative for analysis of fracture resistance of large structures.

Acknowledgment

The fracture testing and data analysis performed by our colleagues Glenn K. Chapman and Dr. Michael J. Morgan are greatly appreciated. This research was supported by the Savannah River Technology Center and the Savannah River Site High Level Waste Division under the Independent R&D Program. The work was funded by the United States Department of Energy under Contract Number DE-AC09-96SR18500.

References

[1] Hancock, J. W., Reuter, W. G. and Parks, D. M., 1993, "Constraint and toughness parameterized by *T*," *Constraint effects in fracture, ASTM STP 1171*, American society of Testing and Materials, Philadelphia, pp. 21-40.

[2] Joyce, J. A. and Link, R. E., 1995, "Effects of constraint on upper shelf fracture toughness," *Fracture Mechanics: 26th Volume, ASTM STP 1256*, American Society for Testing and Materials, Philadelphia, pp. 142-177.

[3] Joyce, J. A. and Link, R. E., 1997, "Application of two parameter elastic-plastic fracture mechanics to analysis of structures," *Engineering Fracture Mechanics*, **57**, pp.431-446.

[4] Marschall, C. W., Papaspyropoulos, V. and Landow, M. P., 1989, "Evaluation of attempts to predict large-crack-growth J-R curves from small specimen tests," Nonlinear Fracture Mechanics: Volume II – Elastic Plastic Fracture, ASTM STP 995, American Society of Testing and Materials, Philadelphia, pp. 123-143.

[5] Eisele, U., Roos, E., Seidenfuss, M. and Silcher, 1992, "Determination of J-integral-based crack resistance curve and initiation values for the assessment of cracked large-scale specimens," Fracture Mechanics: twenty-second symposium (Volume I), ASTM STP 1133, American Society for Testing and Materials, Philadelphia, pp. 37-59.

[6] Roos, E., Eisele, U. and Silcher, H., 1993, "Effect of stress state on the ductile fracture behavior of large scale specimens," *Constraint effects in fracture, ASTM STP 1171*, American Society for Testing and Materials, Philadelphia, pp. 41-63.

[7] Henry, B. S., Luxmoore, A. R. and Sumpter, J. D. G., 1996, "Elastic-plastic fracture mechanics assessment of low constraint aluminum test specimens," International Journal of Fracture, 81, pp. 217-234.

[8] Haynes, M. J. and Gangloff, R. P., 1997, "High resolution *R*-curve characterization of the fracture toughness of thin sheet aluminum alloys," *Journal of Testing and Evaluation*, **25**, pp. 82-98.

[9] Yuan, H. and Brocks, W., 1989, "Numerical investigation on the significant of *J* for large stable crack growth," *Engineering Fracture Mechanics*, **32**, pp.459-468.

[10] Brocks, W., Ebertle, A., Fricke, S. and Veith, H., 1994, "Large stable crack growth in fracture mechanics specimens," *Nuclear Engineering and Design*, **151**, pp. 387-400.

[11] Kikuchi, M., 1997, "Study of the effect of the crack length on the J_{IC} value," *Nuclear Engineering and Design*, 174, pp. 41-49.

[12] Yan, C. and Mai, Y. W., 1997, "Effect of constraint on ductile crack growth and ductile – brittle fracture transition of a carbon steel," *International Journal of Pressure Vessels and Piping*, **73**, pp. 167-173.

[13] Yang, S., Chao, Y. J. and Sutton, M. A., 1993, "Higher order asymptotic crack tip fields in a power-law hardening material," *Engineering Fracture Mechanics*, **45**, pp. 1-20.

[14] Yang, S., Chao, Y. J. and Sutton, M. A., 1993, "Complete theoretical analysis for higher order asymptotic terms and the HRR zone at a crack tip for mode I and Mode II loading of a hardening material," *ACTA MECHANICA*, **98**, pp. 79-98.

[15] Chao, Y. J., Yang, S. and Sutton, M. A., 1994, "On the fracture of solids characterized by one or two parameters: theory and practice," *Journal of the Mechanics and Physics of Solids*, **42**, pp. 629-647.

[16] Chao, Y.J. and Zhu, X.K., 2000, "Constraint-modified *J-R* curves and its applications to ductile crack growth," *International Journal of Fracture*, **106**, pp. 135-160.

[17] Chao, Y. J., Zhu, X. K., Lam, P. S., Louthan, M. R. and Iyer, N. C., 2000, "Application of the two-parameter J-A_2 description to ductile crack growth," *ASTM STP 1389,* G. R. Halford and J. P. Gallagher Eds., American Society for Testing and Materials, Philadelphia, pp. 165-182.

[18] Nikishkov, G. P., Bruckner-Foit, A. and Munz, D., 1995, "Calculation of the second fracture parameter for finite cracked bodies using a three-term elastic-plastic asymptotic expansion," *Engineering Fracture Mechanics*, **52**, pp. 685-701.

[19] Chao, Y.J. and Zhu, X.K., 1998, "J-A_2 Characterization of Crack-Tip Fields: Extent of J-A_2 Dominance and Size Requirements," *International Journal of Fracture*, **89**, pp. 285-307.

[20] Chao, Y.J. and Ji, W., 1995, "Cleavage fracture quantified by J and A_2," *Constraint Effects in Fracture Theory and Applications: Second Volume, ASTM STP 1244*, American Society of Testing and Materials, Philadelphia, pp. 3-20.

[21] Chao, Y. J. and Lam, P. S., 1996, "Effects of crack depth, specimen size, and out-of-plane stress on the fracture toughness of reactor vessel steels," *Journal of Pressure and Vessel Technology*, **118**, pp. 415-423.

[22] Zhu, X. K. and Chao, Y. J., 1999, "Characterization of constraint of fully plastic crack-tip fields in non-hardening materials by the three-term solution," *International Journal of Solids and Structures*, **36**, pp. 4497-4517.

[23] Chao, Y.J., Zhu, X.K. and Zhang, L., 2001, "Higher-order asymptotic crack-tip fields in a power-law creeping material," *International Journal of Solids and Structures*, **38**, pp. 3853-3875.

[24] Kim, Y., Zhu, X.K. and Chao, Y.J., 2001, "Quantification of constraint effect on elastic-plastic 3D crack front fields by the J-A_2 three-term Solution," *Engineering Fracture Mechanics,* **68**, pp. 895-914.

[25] Betegon, C. and Hancock, J. W., 1991, "Two parameter characterization of elastic-plastic crack-tip fields," *Journal of Applied Mechanics*, **58**, pp. 104-110.

[26] O'Dowd, N. P. and Shih, C. F., 1991, "Family of crack-tip fields characterized by a triaxiality parameter – I. Structure of fields," *Journal of the Mechanics and Physics of Solids*. **39**, pp. 989-1015.

[27] O'Dowd, N. P. and Shih, C. F., 1992, "Family of crack-tip fields characterized by a triaxiality parameter – II. Fracture applications," *Journal of the Mechanics and Physics of Solids*. **40**, pp. 939-963.

[28] Hutchinson, J. W., 1968, "Singular Behavior at the End of a Tensile Crack in a Hardening Material," *Journal of the Mechanics and Physics of Solids,* **16**, pp. 13-31.

[29] Hutchinson, J. W., 1968, "Plastic Stress and Strain Fields at a Crack Tip," *Journal of the Mechanics and Physics of Solids*, **16**, pp. 337-347.

[30] Rice, J. R. and Rosengren, G. F., 1968, "Plane Strain Deformation near a Crack Tip in a Power Law Hardening Material," *Journal of the Mechanics and Physics of Solids*, **16**, pp. 1-12.

[31] Chao, Y.J. and Zhang, L., 1997, *Tables of plane strain crack tip fields: HRR and higher order terms*, Me-Report, 97-1, Department of Mechanical Engineering, University of South Carolina, Columbia, South Carolina.

[32] Lam, P. S., 2000, *Comparison of Fracture Methodologies for Flaw Stability Analysis for High Level Waste Storage Tanks*, WSRC-TR-2000-00478, Westinghouse Savannah River Company, Aiken, South Carolina.

Figure Captions

Figure 1. Experimental *J-R* curves for A285 carbon steel SENB and CT specimens

Figure 2. ASTM E 1820 Fracture toughness J_Q for A285 SENB specimen (a/W = 0.32)

Figure 3. ASTM E 1820 Fracture toughness J_Q for A285 SENB specimen (a/W = 0.59)

Figure 4. ASTM E 1820 Fracture toughness J_Q for A285 SENB specimen (a/W = 0.71)

Figure 5. Radial distributions of crack opening stress for SENB and CT specimens

Figure 6. Comparison of predicted and experimental *J-R* curves

Figure 7. Three-dimensional finite element mesh for a cylindrical storage tank

Figure 8. Variation of constraint parameter A_2 with applied pressure and J-integral

Figure 9. Comparison of calculated opening stress and J-A_2 solution

Figure 10. *J-R* curve for A285 storage tank and compared to experimental data

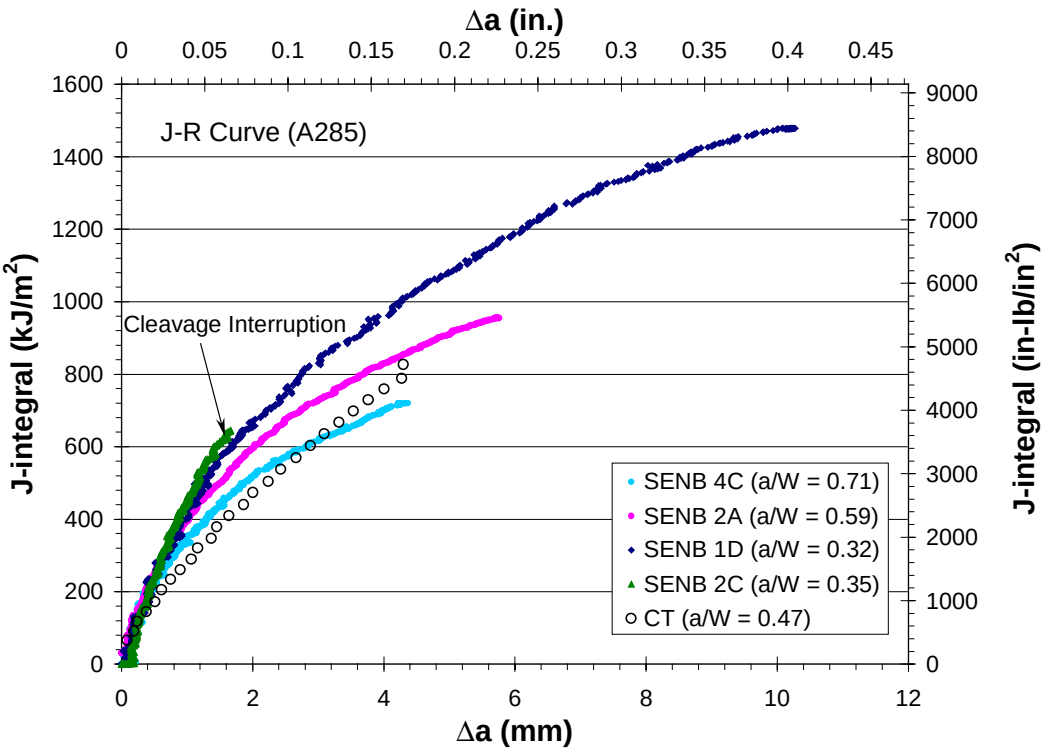

Figure 1. Experimental *J-R* curves for A285 carbon steel SENB and CT specimens

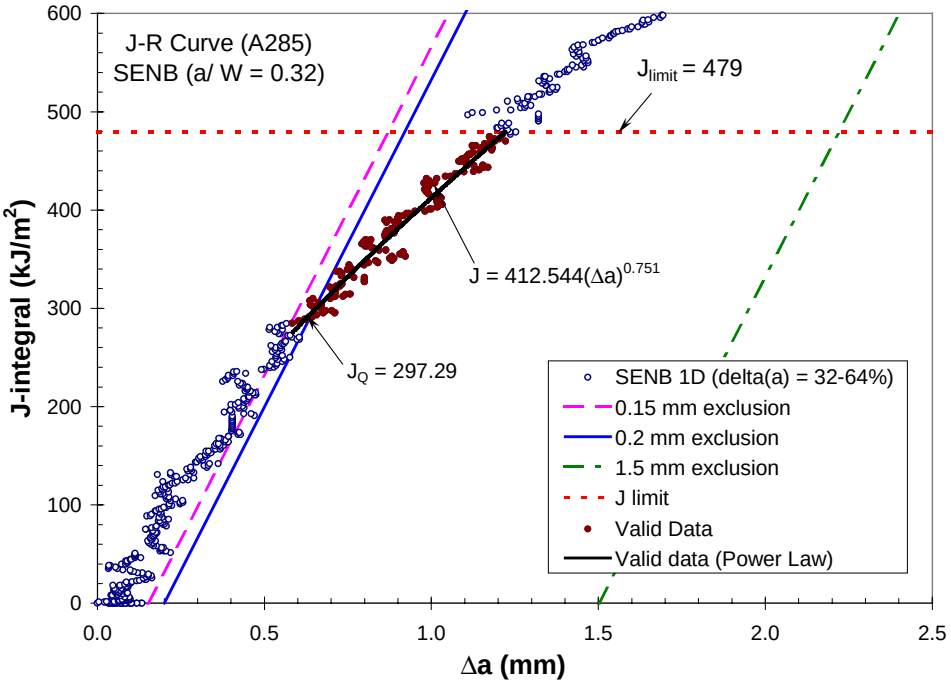

Figure 2. ASTM E 1820 Fracture toughness J_Q for A285 SENB specimen (a/W = 0.32)

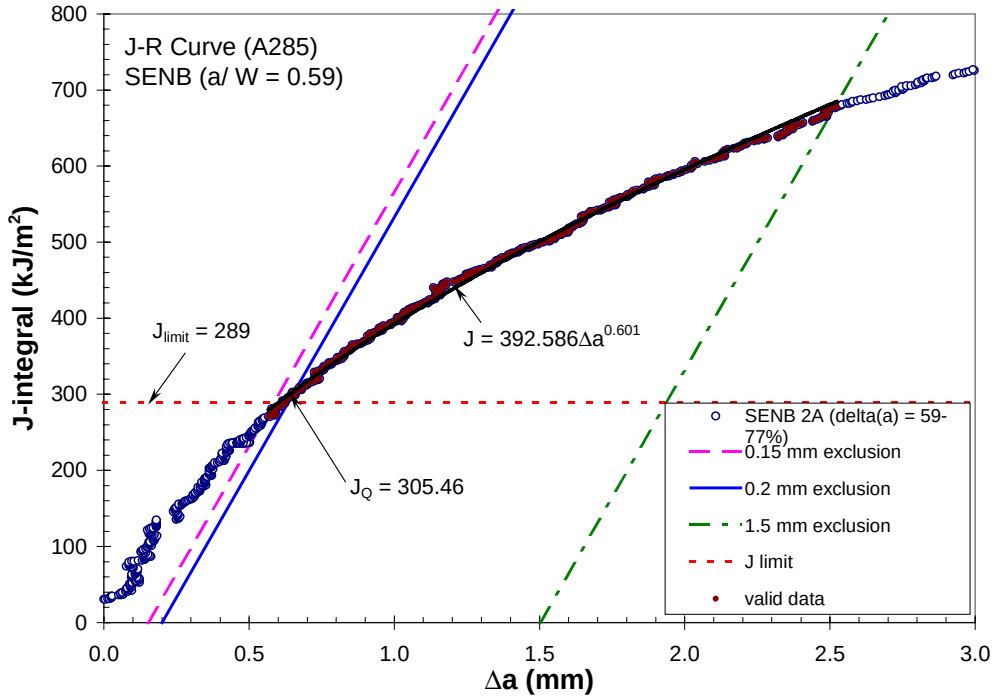

Figure 3. ASTM E 1820 Fracture toughness J_Q for A285 SENB specimen (a/W = 0.59)

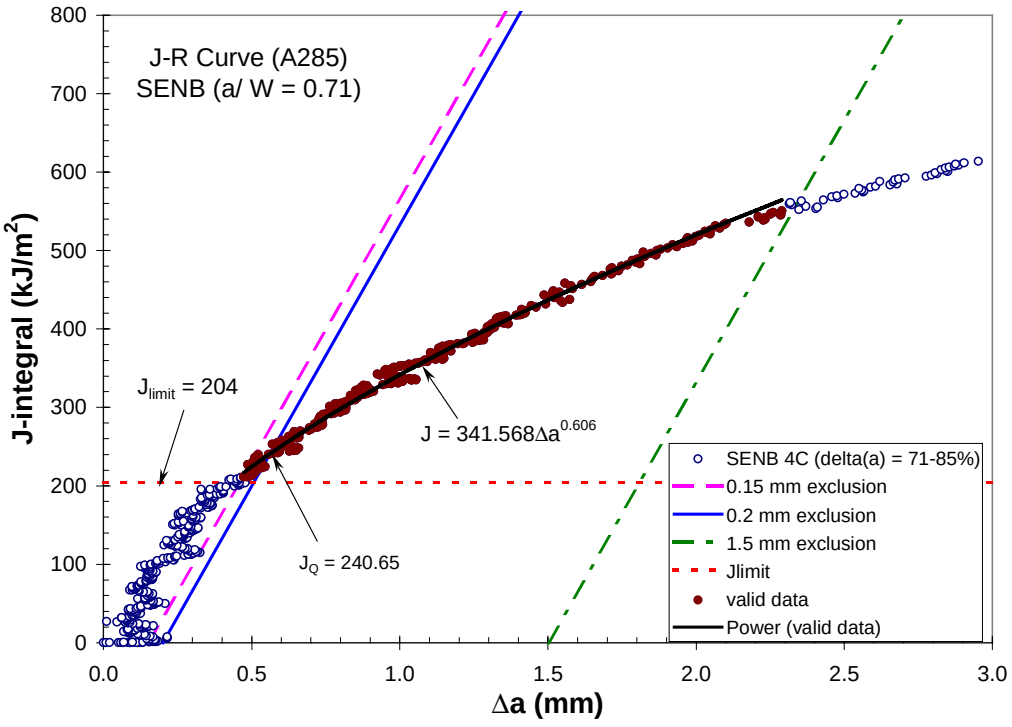

Figure 4. ASTM E 1820 Fracture toughness J_Q for A285 SENB specimen (a/W = 0.71)

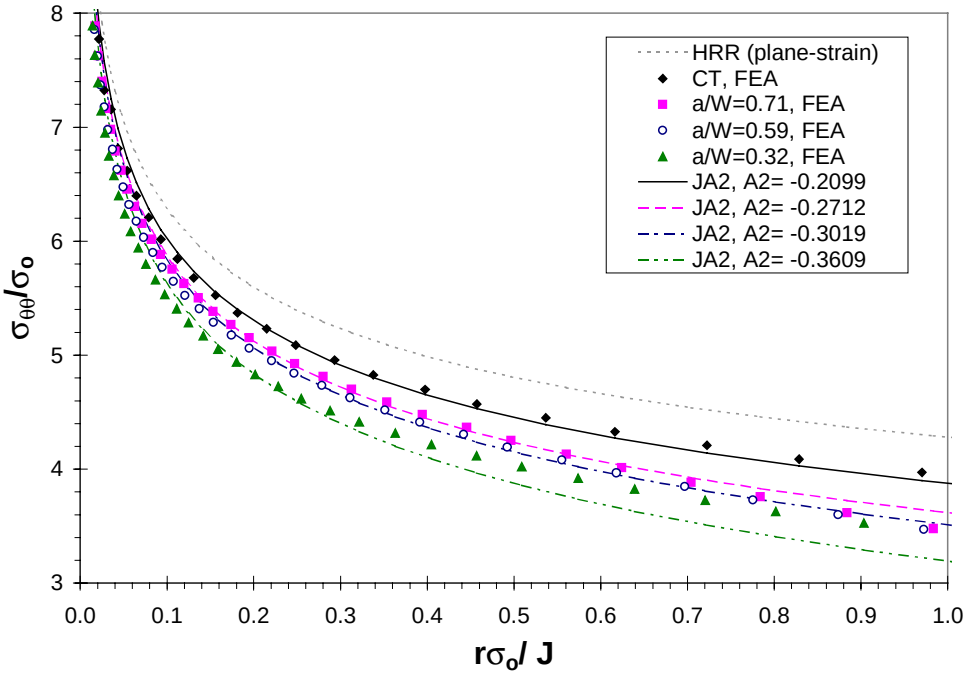

Figure 5. Radial distributions of crack opening stress for SENB and CT specimens

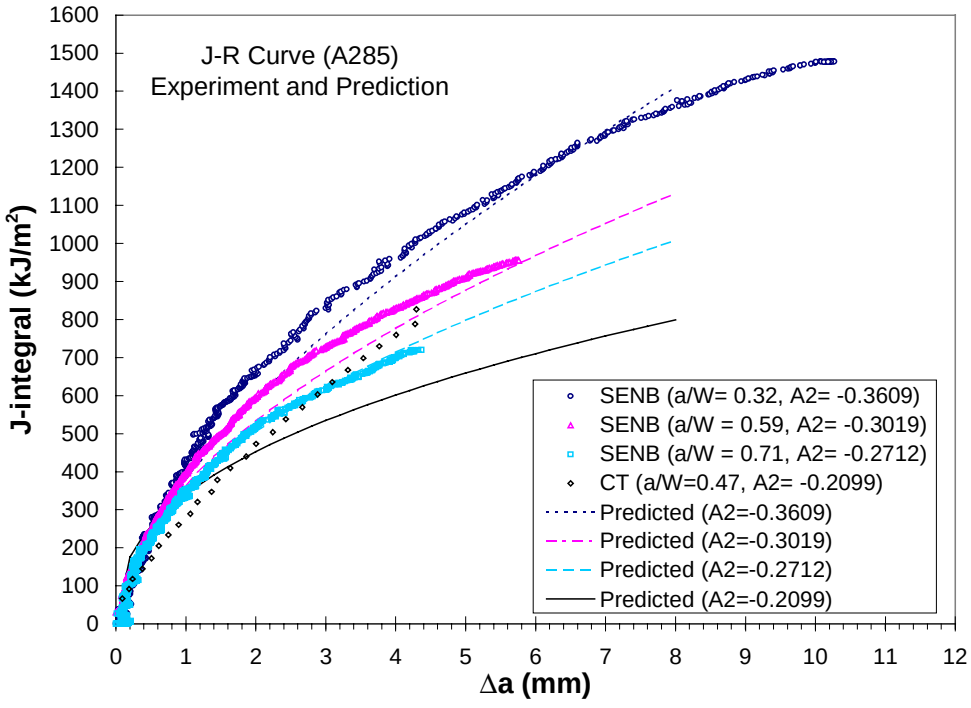

Figure 6. Comparison of predicted and experimental *J-R* curves

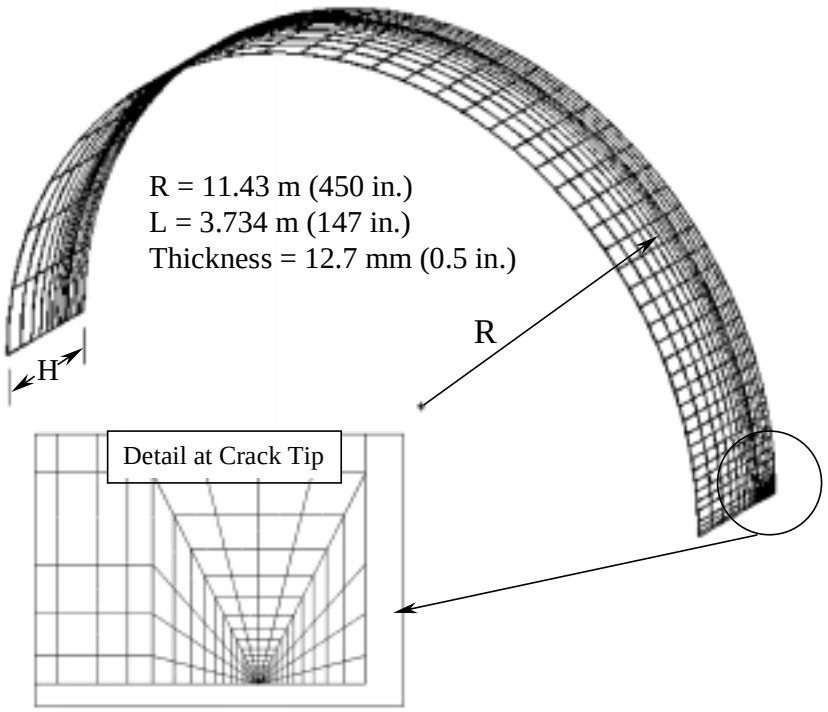

Figure 7. Three-dimensional finite element mesh for a cylindrical storage tank

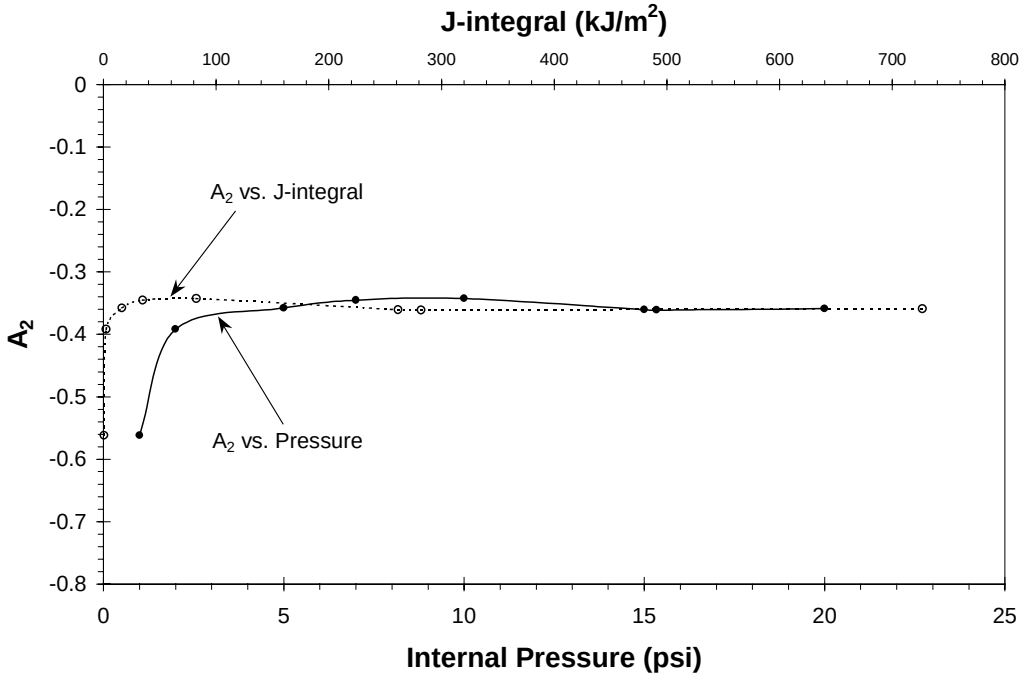

Figure 8. Comparison of calculated opening stress and *J*-A_2 solution

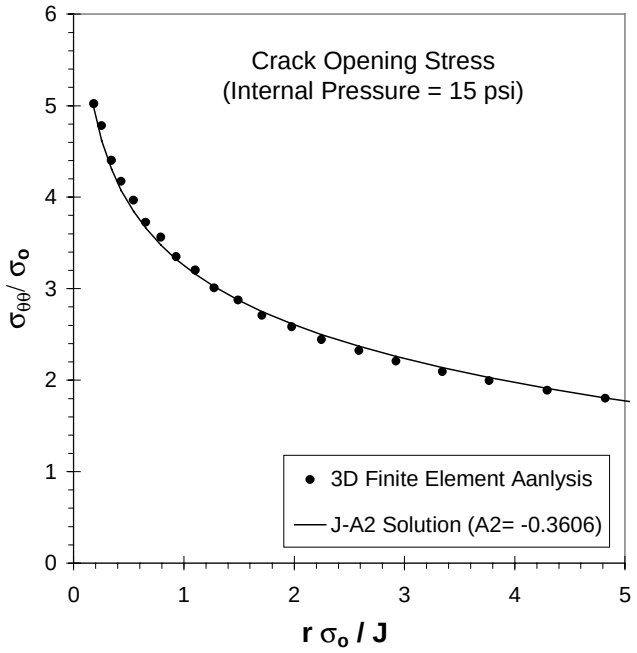

Figure 9. Variation of constraint parameter A_2 with applied pressure and J-integral

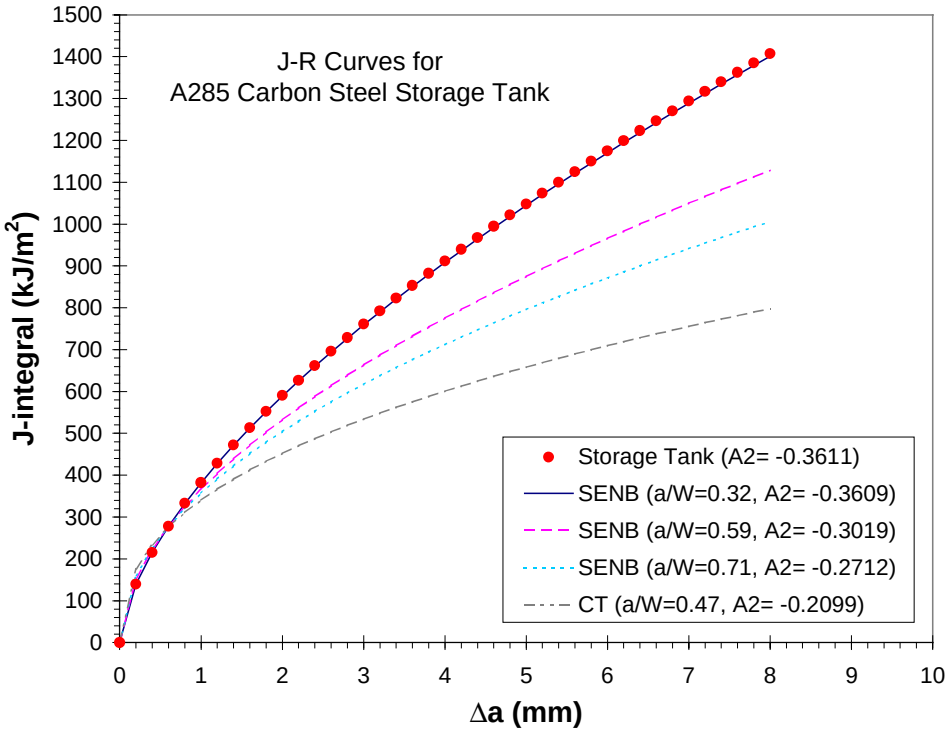

Figure 10. *J-R* curve for A285 storage tank and compared to experimental data